International Journal of Power Electronics and Drive System (IJPEDS)
Vol. 8, No. 1, March 2017, pp. 130~146
ISSN: 2088-8694, DOI: 10.11591/ijpeds.v8i1.pp130-146

Experimental Comparison between Four and Six Switch Inverters Fed FLC Based Speed Sensorless IM Drives at Very Low Speed

Z. M. S. Elbarbary
Department of Electrical Engineering, Kaferelsheihk University- Egypt
Department of Electrical Engineering, King Khalid university-KSA

Article Info

Article history:

Received Oct 01, 2016
Revised Dec 07, 2016
Accepted Dec 17, 2016

Keyword:

Digital signal processor
Four switch inverter
Fuzzy logic control
Induction motor
Sensorless control
Six switch inverter

ABSTRACT

This paper introduces experimental comparison study between six and four switch inverter fed three phase induction motor drive system. The control strategy of the drive is based on speed sensoreless vector control using model reference adaptive system as a speed estimator. The adaptive mechanism of speed control loop depends on fuzzy logic control. Four switch inverter conFigureurations reduces the cost of the inverter, the switching losses, the complexity of the control algorithms, interface circuits, the computation of real-time implementation, volume-compactness and reliability of the drive system. The robustness of the proposed model reference adaptive system based four switch three-phase inverter (FSTPI) fed induction motor drive is verified experimentally at different operating conditions. Experimental work is carried using digital signal processor (DSP1103) for a 1.1 kW motor. A performance comparison of the proposed FSTP inverter fed IM drive with a conventional six switch three-phase inverter (SSTP) inverter system is also made in terms of speed response. The results show that the proposed drive system provides a fast speed response and good disturbance rejection capability. The proposed FSTP inverter fed IM drive is found quite acceptable considering its performance, cost reduction and other advantages features.

Corresponding Author:

Zakaria Mohamed Salem,
Department of Electrical Engineering,
Kaferelsheikh University Kaferelsheikh,
Egypt.
Email: z_elbarbary@yahoo.com

1. INTRODUCTION

Induction motors are called the workhorse of the motion industry because they are most widely used motors for appliances, industrial control, and automation. They are robust, reliable, simple, cheap and available in all power ratings. The squirrel cage types of induction motors are very popular in variable-speed drives. When AC power is supplied to an induction motor at certain specifications, it runs at its rated speed. However, many applications need variable speed operations. Due to the progress in the field of semiconductor i.e. power electronics and integrated circuits enables the application of induction motors for high-performance drives. These power electronics not only control the motor's speed, but can improve the motor's dynamic and steady state characteristics. In addition, this improves the energy savings and reduces noise generation of the motor. Induction motor drives have been thoroughly studied in the past few decades and many vector control strategies have been proposed, ranging from low cost to high performance applications. Traditionally, 6-switch, 3-phase (SSTP) inverters have been widely utilized for variable speed

IM drives. This involves the losses of the six switches as well as the complexity of the control algorithms and interface circuits to generate six PWM logic signals [1]-[3].

In the past, researchers mainly concentrated on the development of the efficient control algorithms for high performance variable speed IM drives However, the cost, simplicity and flexibility of the overall drive system which become some of the most important factors did not get that much attention to the researchers. That's why, despite tremendous research in this area most of the developed control system failed to attract the industry [4]-[5].

Usually, high performance motor drives used in robotics, rolling mills, machine tools, etc. require fast and accurate response, quick recovery of speed from any disturbances and insensitivity to parameter variations. The dynamic behavior of an AC motor can be significantly improved using vector control theory where motor variables are transformed into an orthogonal set of d-q axes such that speed and torque can be controlled separately. This gives the IM machine the highly desirable dynamic performance capabilities of a separately excited DC machine, while retaining the general advantages of the AC over DC motors [6]-[8].

In this paper, a cost effective FSTP inverter fed sensorless IM drive is developed. The four switches makes the inverter less cost, less switching losses, less chances of destroying the switches due to lesser interaction among switches, less complexity of control algorithms and interface circuits as compared to the conventional SSTP inverter, the proposed control approach reduces the computation for real time implementations. Furthermore, the use of speed sensorless for induction motor drives besides being reduce bulky and increase the robustness, it reduce additional electronics, extra wiring, extra space and reduce extra cost to the drive system,speed sensor, also, implies and careful mounting which detracts from the inherent robustness of the drive.

The proposed sensorless control method verifies the validity of an MRAS-based FSTP inverter fed IM drive system for cost reduction and other previously mentioned advantages Thus, the main issue of this paper is to analyse a cost effective, simple and efficient high performance IM drive. The performance of a closed-loop vector control scheme of the proposed FSTP inverter fed IM speed sensorless drive is implemented using digital signal processing DSP1103 interfaced with the MATLAB/SIMULINK software.

2. DRIVE SYSTEM

The proposed system intended for performance analysis of speed sensorless indirect rotor field oriented control of induction motor drive is shown in Figure 1. It consists of IM, inverter, speed estimation algorithm and speed controller. The estimated motor speed is compared with the speed command and the produced error is used to drive a fuzzy logic based PI-controller. The output of the controller is a torque command. The field oriented control (FOC) block receives the torque command T*, while the flux command λ_{dr}^{*} is maintained constant. The field oriented control block performs the slip calculation equation (1) and generates the current command components i_{qs}^{e} *and* i_{ds}^{e} in a rotating reference frame, equations (2 to 5) respectively. These components are further manipulated by axes transformations to obtain the abc current command components iar, ibr, and icr. Using park's transformation These current command components are used as references of current control of the inverter. The slip speed calculated as follow:

$$\omega_{sl}^{*} = \frac{L_m}{T_r^{*}} \cdot \frac{I_{qs}^{e*}}{\lambda_{dr}^{e*}} \tag{1}$$

D-axis current component is calculated as follow:

$$I_{ds}^{e*} = \frac{1}{L_m}(1 + T_r^{*} p)\lambda_{dr}^{e*} \tag{2}$$

Angular frequency is obtained as follows,

$$\omega_e = \omega_r + \omega_{sl} \tag{3}$$

$$\theta_e = \int \omega_e . dt \tag{4}$$

The torque producing current component is calculated from:

$$I_{qs}^{e*} = \frac{1}{k_t}\frac{(\omega_r^* - \omega_r)}{\lambda_{dr}^{e*}}\frac{K_{ps}[1+\tau_{cs}S]}{\tau_{cs}S} \quad (5)$$

Where ω_r is the motor estimated speed.

A comparison of the proposed FSTP inverter fed IM drive with a conventional SSTP inverter system is also made experimentally in term of total harmonic distortion (THD) of the stator current and speed response. The proposed inverter fed IM drive is found good considering its cost reduction and other advantages.

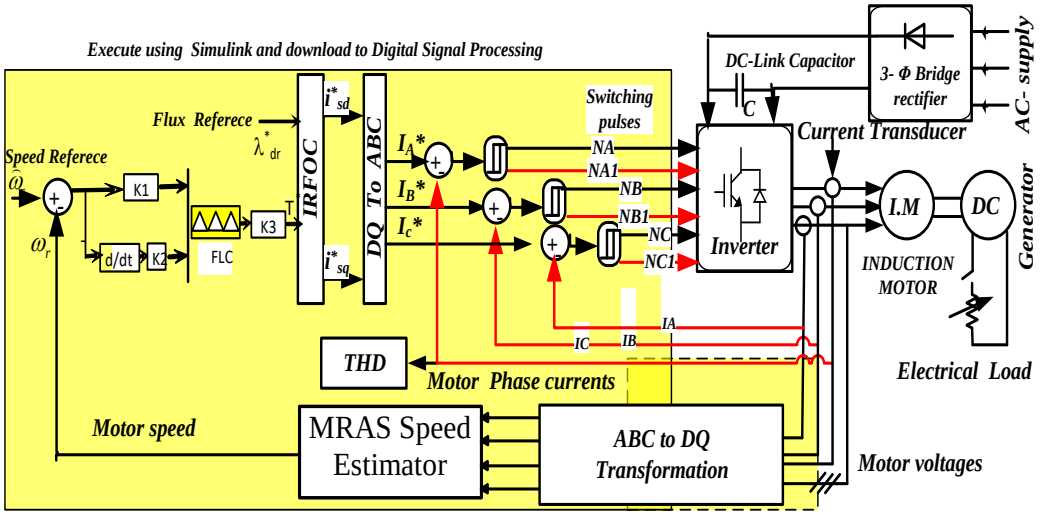

Figure 1. Overall block diagram of three-phase induction drive system based on vector control theory

2.1. Fuzzy based pi controller design

Traditional control systems are usually based on a definite mathematical model often represented by a set of differential equations which describe the relation between input and output variables as well as the system parameters. In contrast, fuzzy logic controller does not require such precise mathematical model. A fuzzy logic controller consists typically of three stages or blocks namely, input block, processing block, and output block as illustrated by Figure 2. The input block converts input signals into appropriate way to pertinence functions. The processing block invokes appropriate rules, generates a result for each rule, and combines the results of those rules. Finally, the output block transforms the combined result into a control signal [9],[10].

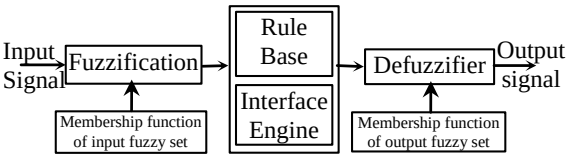

Figure 2. Fuzzy control system

The fuzzy logic PI controller is illustrated in Figure 3, in which KP = Ku R(Kde) and KI = KuR(Ke) are the controller proportional and integral gains. The functions R(Kde) and R(Ke) are defined by the controller rule base which is summarized in Table 1. Initially the fuzzy input vector should be defined. It consists of two variables; the speed error and its derivative as explained in equations (6) ad (7):

$$e(t) = \omega_r^* - \omega_r \quad (6)$$

$$\frac{d}{dt}e(t) = \frac{d}{dt}(\omega_r^* - \omega_r) \tag{7}$$

A fuzzy set for input and output variables is designed. Figure 4 and 5 show the five linguistic variables used for each fuzzy input variable, while the output variable fuzzy set is shown in Figure 6. The linguistic variables (LV's) used for inputs shown in Figures 4 and 5 are PB (Positive Big); PS (Positive Small); ZE (Zero); NB (Negative Big); and NS (Negative Small). The same LV's are used for the output fuzzy set shown in Figure 6.

If (Input1 AND Input2) THEN Output

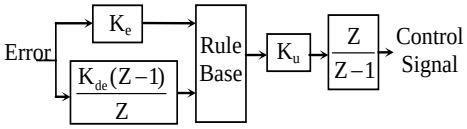

Figure 3. Fuzzy logic PI controller

A look-up table is required to develop the set of rules, in which the relation between the input variables, $e(t)$ and $\frac{d}{dt}(e(t))$ are defined and the output variable of fuzzy logic controller can be obtained. The look-up table used in the simulation program is given in Table 1. The output depends on the fuzzy rule expressed as follows;

Table 1. Fuzzy rule

		Error				
		NS	NB	ZE	PB	PS
Error rate of change	NS	NS	NS	NS	NP	ZE
	NB	NS	NS	NB	ZE	PB
	ZE	NS	NB	ZE	PB	PS
	PB	NB	ZE	PB	PS	PS
	PS	ZE	PB	PS	PS	PS

In this section, the FLC controller is considered which has two-input and one-output. IF-THEN rules used in the formulation of the knowledge base, these IF-THEN rules have the following form shown in Figure 4 and Figure 5, respectively. The fuzzy system considered here has following specifications: Singleton fuzzifier, triangular membership functions for each input, and for the output.

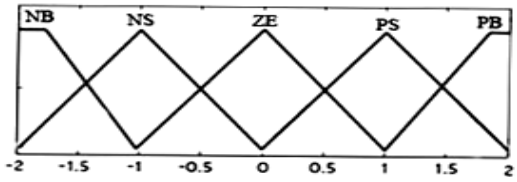

Figure 4. Error Memberships

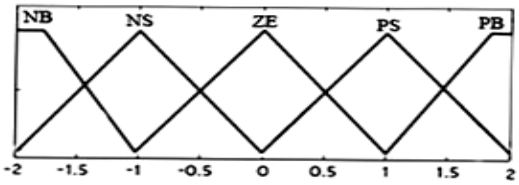

Figure 5. Rate of Change of Error

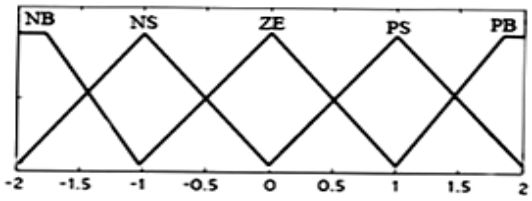

Figure 6. Output membership

2.2. Mathematical model of three-phase IM

Squirrel-cage Three-phase induction motor is represented in its d-q synchronous reference frame. The winding axes of three-stator winding are displaced by 120 electrical degrees. In this analysis the air gap is uniform and the windings are sinusoidally distributed around the air gap. Magnetic saturation and core losses are neglected. The well-known d-q rotating reference is used in analysis and control. The three-phase induction machine can be modeled with the following voltage equations in synchronous reference frame [9]. The stator quadrature-axis voltage is given by:

$$V_{qs} = R_s i_{qs} + s\psi_{qs} + \omega\psi_{ds} \tag{8}$$

$$V_{ds} = R_s i_{ds} + s\psi_{ds} + \omega\psi_{qs} \tag{9}$$

For the stationary reference frame ω = 0, substitute into Equations (8) and (9) yields:

$$V_{qs} = R_s i_{qs} + s\psi_{qs} \tag{10}$$

$$V_{ds} = R_s i_{ds} + s\psi_{ds} \tag{11}$$

The stator q-axis flux linkage is given by:

$$\begin{aligned} \psi_{qs} &= L_s i_{qs} + L_m i_{qr} \\ &= (L_{ls} + L_m) i_{qs} + L_m i_{qr} \\ \psi_{qs} &= L_{ls} i_{qs} + L_m (i_{qr} + i_{qs}) \end{aligned} \tag{12}$$

The stator d-axis flux linkage is given by:

$$\begin{aligned} \psi_{ds} &= L_s i_{ds} + L_m i_{dr} \\ &= (L_{ls} + L_m) i_{ds} + L_m i_{dr} \\ \psi_{ds} &= L_{ls} i_{ds} + L_m (i_{dr} + i_{ds}) \end{aligned} \tag{13}$$

In matrix form,

$$\begin{bmatrix} V_{qse}^e \\ V_{dse}^e \\ 0 \\ 0 \end{bmatrix} = \begin{bmatrix} R_s + pL_\sigma & \omega_e L_\sigma & p\frac{L_m}{L_r} & \omega_e \frac{L_m}{L_r} \\ -\omega_e L_\sigma & R_s + pL_\sigma & -\omega_e \frac{L_m}{L_r} & p\frac{L_m}{L_r} \\ -R_r L_m & 0 & R_r + pL_\sigma & (\omega_e - \omega_r) L_m \\ 0 & -R_r L_m & -(\omega_e - \omega_r) L_m & R_r + pL_\sigma \end{bmatrix} \begin{bmatrix} I_{qs}^e \\ I_{ds}^e \\ \Psi_{qr}^e \\ \Psi_{dr}^e \end{bmatrix} \tag{14}$$

The electromagnetic torque is given by:

$$T_e = \frac{3}{2}\frac{p}{2}(\psi_{ds} i_{qs} - \psi_{qs} i_{ds}) \tag{15}$$

$$T_e - T_l = j\frac{d\omega}{dt} + B\omega \tag{16}$$

2.3. Three-phase inverter

In this work, the inverter switches are considered as ideal power switches and it is assumed that the conduction state of the power switches is associated with binary variables Therefore; a binary "1" will indicate a closed state, while "0" will indicate the open state.

2.3.1. Six-Switch three thase inverter

The conventional three phase inverter is conFigured with six switches S_1, S2, S3, S4, S5 and S6, respectively, as shown in Figure 7.

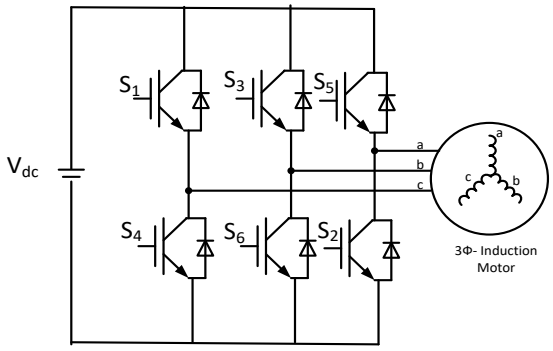

Figure. 7 Six-switches three-phase inverter topology

The inverter converts the DC-voltage to a balanced three-phase output with adjustable voltage and frequency. The output voltages are introduced as a function of switching logic by the following equation:

$$V_a = \frac{V_{dc}}{3}(2NA - NB - NC). \tag{17}$$

$$V_b = \frac{V_{dc}}{3}(2NB - NA - NC). \tag{18}$$

$$V_c = \frac{V_{dc}}{3}(2NC - NB - NA). \tag{19}$$

In matrix form,

$$\begin{bmatrix} V_a \\ V_b \\ V_c \end{bmatrix} = \frac{V_{dc}}{3}\begin{bmatrix} 2 & -1 & -1 \\ -1 & 2 & -1 \\ -1 & -1 & 2 \end{bmatrix}\begin{bmatrix} NA \\ NB \\ NC \end{bmatrix} \tag{20}$$

2.3.2. Four-switch three phase inverter

In four switch (S1 to S4) inverter the center point of the capacitors forms the third phase "c", as shown in Figure 8. The current in phase "c" is the result of the currents in the two controlled phases. A detailed comparison of the four-switch inverter with the conventional six-switch inverter conFigureuration is given in [11]-[14]. Two control possibilities exist to control the four-switch bridge inverter, i.e., two- level current control to force the two controlled phases currents to be sinusoidal, or using PWM to control the voltages applied to the three-phase quasi sinusoidally. The two level current control of the four-switch bridge inverter used to control the load current by forcing it to follow a reference one. This is achieved by the switching action of the inverter to keep the current within the hysteresis band. The load currents are sensed and compared with respective command currents using two independent hysteresis comparators. The output signals of the comparators are used to activate the inverter power switches. This controller is simple and provides excellent dynamic performance.

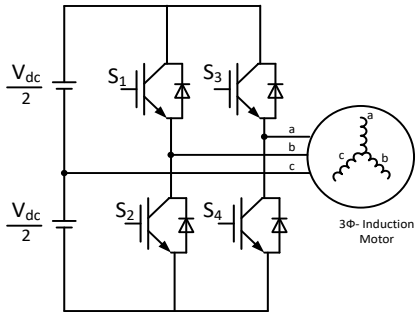

Figure 8. Four-switches three-phase inverter topology

The modulated phase's voltages of four switch inverter are introduced as a function of switching logic NA, NA1, NB and NB1 of power switches by the following relations.

$$V_a = \frac{0.5V_{dc}}{6}(4NA + 2.NB - 1). \quad (21)$$

$$V_b = \frac{0.5V_{dc}}{6}(-2NA + 4.NB - 1). \quad (22)$$

$$V_c = \frac{0.5V_{dc}}{6}(-2NA - 2.NB + 2). \quad (23)$$

In matrix form,

$$\begin{bmatrix} V_a \\ V_b \\ V_c \end{bmatrix} = \frac{V_{dc}}{6}\begin{bmatrix} 4 & 2 & -1 \\ -2 & 4 & -1 \\ -2 & -2 & 2 \end{bmatrix}\begin{bmatrix} NA \\ NB \\ 1 \end{bmatrix} \quad (24)$$

Where, NA1 and NB1 are complementary of NA and NB, Also, it will be assumed that a stiff voltage is available across the two dc-link capacitors.

2.4. Speed estimator based on MRAS

Model Reference Adaptive Systems (MRAS) techniques are applied in order to estimate rotor speed. This technique is based on the comparison between the outputs of two estimators. The outputs of two estimators may be (the rotor flux, back emf, or motor reactive power). The estimator that does not involve the quantity to be estimated (The rotor speed ωr) is considered as the induction motor voltage model. This model is considered to be the reference model (RM). The other model is the current model, derived from the rotor equation, this model considered to be the adjustable model (AM). The error between the estimated quantities by the two models is used to drive a suitable adaptation mechanism which generates the estimated rotor speed [15]-[17]. In this paper, the observer depends on model reference adaptive system (MRAS) technique. The speed observer is based on stator current and rotor flux as state variables as show in Figure 9 [18].

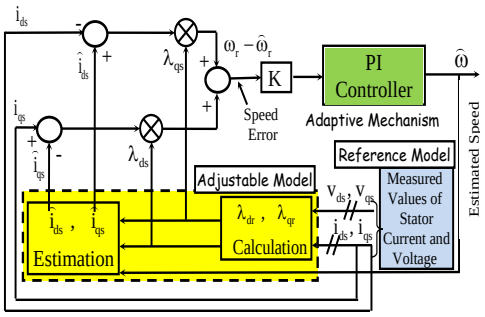

Figure 9. Block Diagram for the Speed Estimation Procedure

The speed estimating procedures from the stator current error are as follows: From the induction motor equation the stator current is represented as:

$$\begin{aligned} i_{ds} &= \frac{1}{Lm}\left[\psi_{dr} + \omega_r T_r \psi_{qr} + T_r p\psi_{dr}\right] \\ i_{qs} &= \frac{1}{Lm}\left[\psi_{qr} - \omega_r T_r \psi_{qr} + T_r p\psi_{qr}\right] \end{aligned} \tag{25}$$

Using Equation (23), and estimated instead of measured speed, the stator current is estimated as:

$$\begin{aligned} \hat{i}_{ds} &= \frac{1}{Lm}\left[\psi_{dr} + \hat{\omega}_r T_r \psi_{qr} + T_r p\psi_{dr}\right] \\ \hat{i}_{qs} &= \frac{1}{Lm}\left[\psi_{qr} - \hat{\omega}_r T_r \psi_{qr} + T_r p\psi_{qr}\right] \end{aligned} \tag{26}$$

Form the relationship between the real stator current and the estimated stator current, the difference in the stator current is obtained as

$$\begin{aligned} i_{ds} - \hat{i}_{ds} &= \frac{T_r}{Lm}\psi_{qr}\left[\omega_r - \hat{\omega}_r\right] \\ \hat{i}_{qs} - i_{qs} &= \frac{T_r}{Lm}\psi_{dr}\left[\omega_r - \hat{\omega}_r\right] \end{aligned} \tag{27}$$

The difference between estimated and measured values of stator current is sinusoidal because it is the function of rotor flux.

$$\begin{aligned} (i_{ds} - \hat{i}_{ds})\psi_{qr} &= \frac{T_r}{Lm}\psi_{qr}^2\left[\omega_r - \hat{\omega}_r\right] \\ (\hat{i}_{qs} - i_{qs})\psi_{dr} &= \frac{T_r}{Lm}\psi_{dr}^2\left[\omega_r - \hat{\omega}_r\right] \end{aligned} \tag{28}$$

By summing the above two equations.

$$(i_{ds} - \hat{i}_{ds})\psi_{qr} + (\hat{i}_{qs} - i_{qs})\psi_{dr} = \frac{T_r}{Lm}(\psi_{qr}^2 + \psi_{dr}^2)\left[\omega_r - \hat{\omega}_r\right] \tag{29}$$

Hence, the error of the rotor speed is obtained as follows:

$$\begin{aligned} &\omega_r - \hat{\omega}_r = [(i_{ds} - \hat{i}_{ds})\psi_{qr} - (i_{qs} - \hat{i}_{qs})\psi_{dr}] / K \\ &\textit{Where} \qquad K = \frac{T_r}{Lm}(\psi_{qr}^2 + \psi_{dr}^2) \end{aligned} \tag{30}$$

The right hand term seems as the term of speed calculation from adaptive observer, so the speed can be calculated from the following equation:

$$\begin{aligned} \hat{\omega}_r = \frac{1}{K}[&(K_p(i_{ds} - \hat{i}_{ds})\psi_{qr} - (i_{qs} - \hat{i}_{qs})\psi_{dr}) + \\ &(K_I\int(i_{ds} - \hat{i}_{ds})\psi_{qr} - (i_{qs} - \hat{i}_{qs})\psi_{dr})] \end{aligned} \tag{31}$$

2.5. Expermental setup and results

To verify the validity of the proposed system, an induction motor drive system was constructed. Figure 10 shows a block diagram of the experimental system, it consists of three-phase squirrel cage induction machine coupled to a separately excited DC generator working as a load. The machine under test was operated under speed sensorless indirect rotor field-oriented control.

The parameters of the machine under test are given in the Appendix. The control is done on a digital signal processor controller board (DSP 1103), which is based on 32-bit floating point DSP TI TMS32OC3I. This board is plugged into a host computer. It performs the speed sensorless vector control algorithm, and the

hysteresis current controller generates the pulse sequences for the switches of three-phase voltage source inverter. There is a communication board for transferring and receiving data between the control algorithm on the DSP 1103 and the real-time system. Two phases currents and voltages Ia, Ib and Va,Vb are sensed by Hall-effect current and voltage transducers. These signals are fed to the DSP through the signal conditioning circuit. An optional speed signal of the rotor is available by using 2048 pulse/revolution incremental encoder; this signal of the motor speed is fed to the encoder interface on the DSP board.

The control algorithm is executed by 'Matlab/simulink' and down loaded to the board through host computer. The outputs of the board are six logic signals, which are fed to the, 3-phase inverter through driver circuits. The sampling time for mental implementation is chosen as 100 sec. The performance of the conventional six switch inverter based MRAS speed sensorless IM drive system and four-switch based system are compared at different operating conditions experimentally I the following subsections.

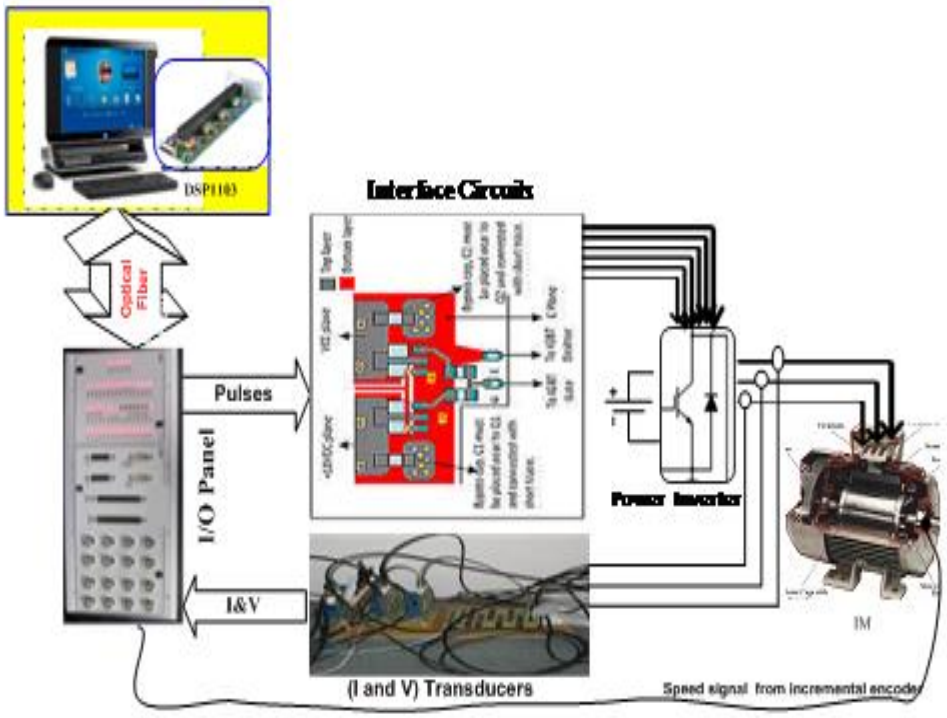

Figure 10. Experimental-setup

2.5.1. Speed step down change from 80 To 60 rad/sec at full load

The response due to a step change in the speed command is used to evaluate the performance in terms of transient and steady state errors also, stability of speed estimation algorithm for both no load and full load conditions are explained. Figure 11 shows the estimated and measured speed response with a command speed step down change from 80 to 60 rad/sec at full load of four switch inverter based drive system. Figure 11A shows the measured and estimated speed with its speed reference, both estimated and measured speed signals is decelerated smoothly to follow its reference value with nearly zero steady state error which means good speed estimation. Figure 11B shows the difference between the estimated and measured speed, it is closed to zero. Figure 11C shows the motor phase current with its reference, it is noted that the current follows its reference during speed step down change. Figure 11D shows the motor three phase currents, the currents frequency decrease with decreasing speed.

In order to provide a fair comparison between conventional SSTP and FSTP when fed senseless induction motor drive system, the results of speed step change response of the SSTP inverter fed IM drive at the same condition of FSTP inverter is presented in Figure 12. Figure 12A shows the estimated and measured speed signals which follow its reference speed. Figure 12B shows the speed difference between the estimated and measured speed, the error between two signals is closed to zero Figure 12C shows the motor phase current whereas Figure 12D shows three phase motor currents for the step down change in speed command.

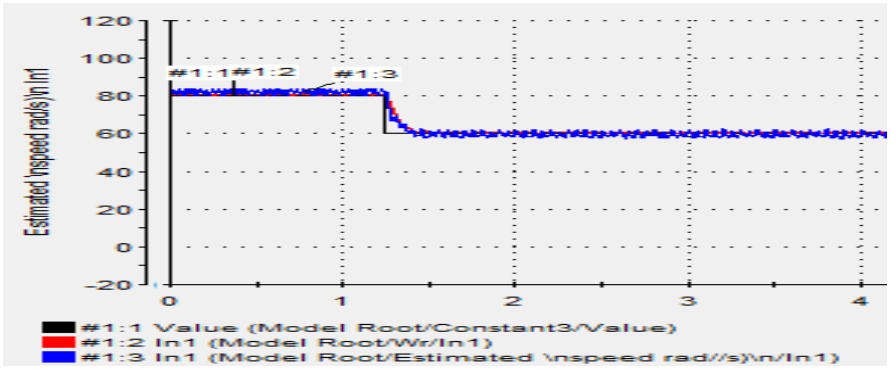

(A)

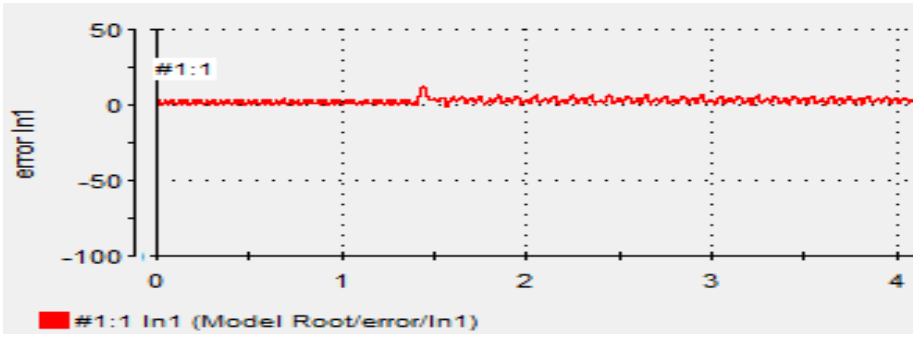

(B)

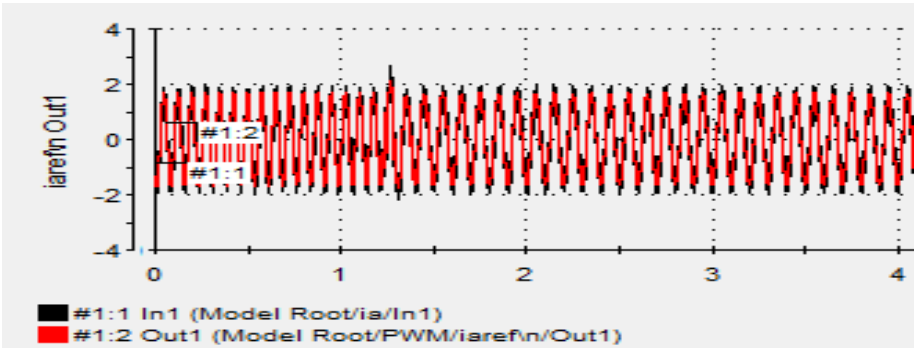

(C)

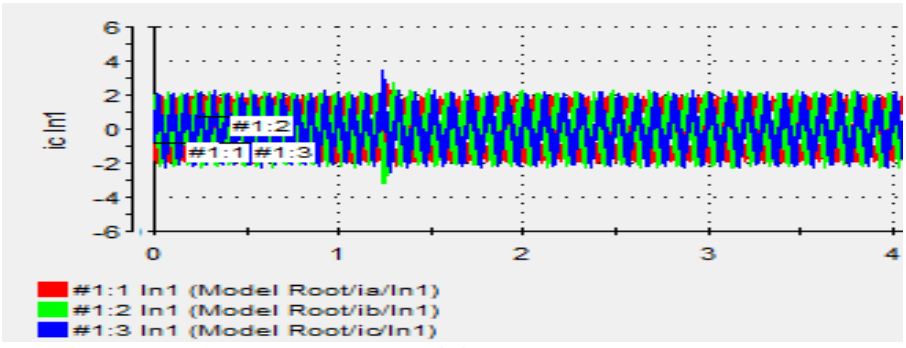

(D)

Figure 11. Speed Step down change of FSTPI drive (from 80 to 60 rad/ sec at Full load) Experimental results of FSTPI drive: (A) motor speed, (B) speed error (C) phase current, (D) three-phase currents

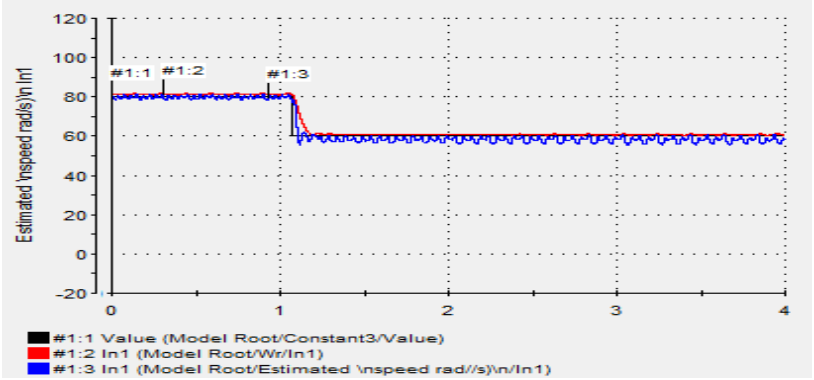

(A)

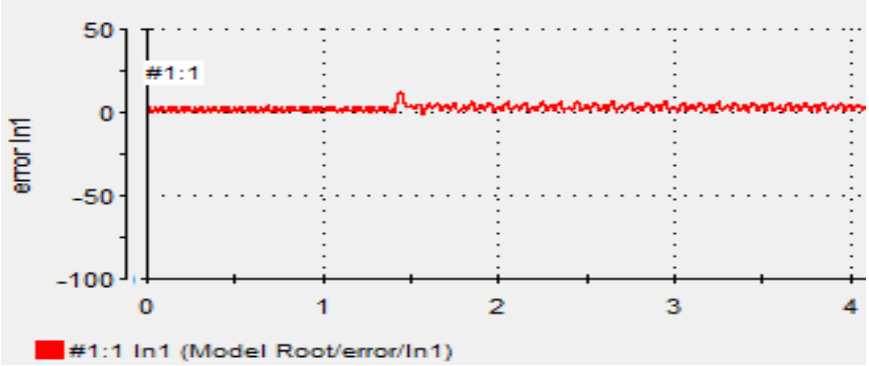

(B)

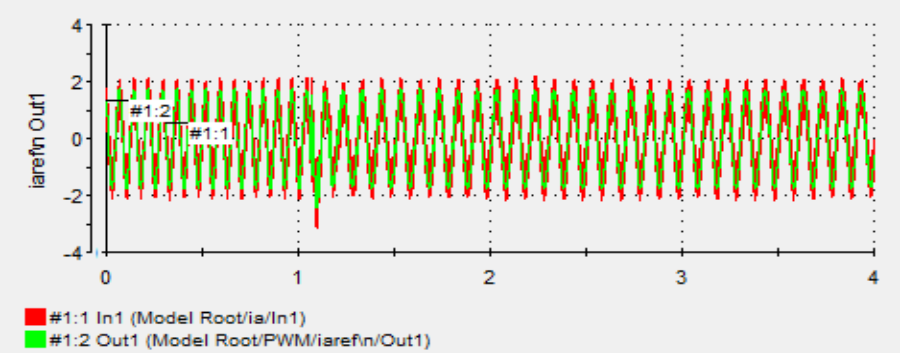

(C)

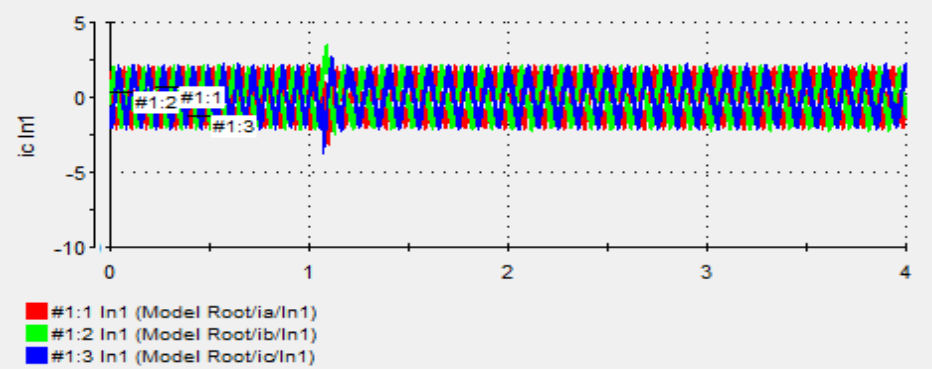

(D)

Figure 12. Speed Step down change of SSTPI drive (from 80 to 60 rad/ sec at Full load) Experimental results of SSTPI drive: (A) motor speed, (B) speed error (C) phase current, (D) three-phase currents

2.5.2. Speed step up change from 40 to 60 rad/sec at full load

Another case to study is the drive response, is speed step up change at full load from 40 to 60 rad/sec. Figure 13 shows the drive response when motor fed from FSTP inverter. The motor is running at 40 rad/sec, At t=1.25 sec, the speed reference has been changed to 60 rad/sec. Figure 13A shows that perfect speed tracking with zero steady state error. The response indicates how well the controller succeeds in forcing the actual rotor speed to follow the desired reference trajectory with nearly zero steady-state error. Figure 13B shows the speed error which is much close to zero. Figure 13C shows the motor phase current, whereas Figure 13D shows the motor three phase current, it frequency increases with step up of speed reference. Figure 14 shows three phase motor current with good shape of sine wave. Figure 14 shows the drive response when fed from SSTPI. Speed signals shown in Figure 14A with good correlation between measured and estimated speed signals. Figure 14B shows the speed error, it's very close to zero. Figure 14C shows motor phase current with its reference. Figure 14D shows three phase motor currents.

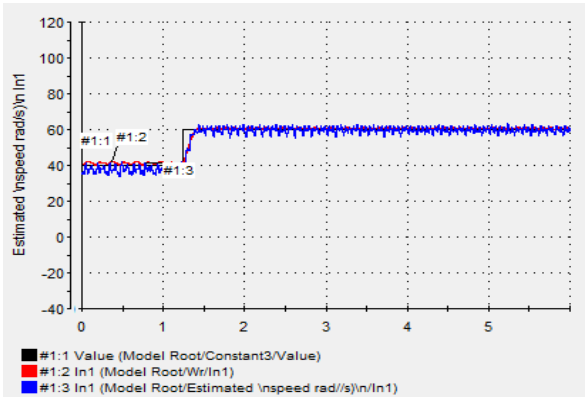

(A)

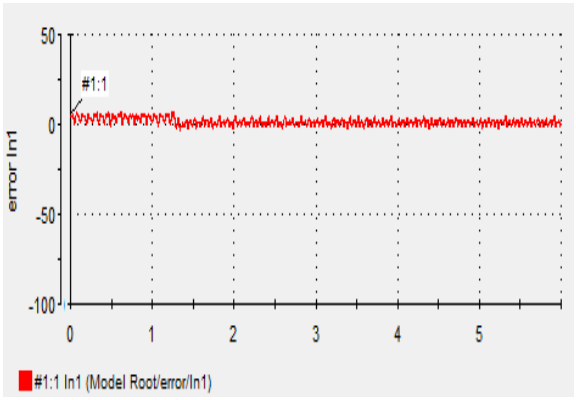

(B)

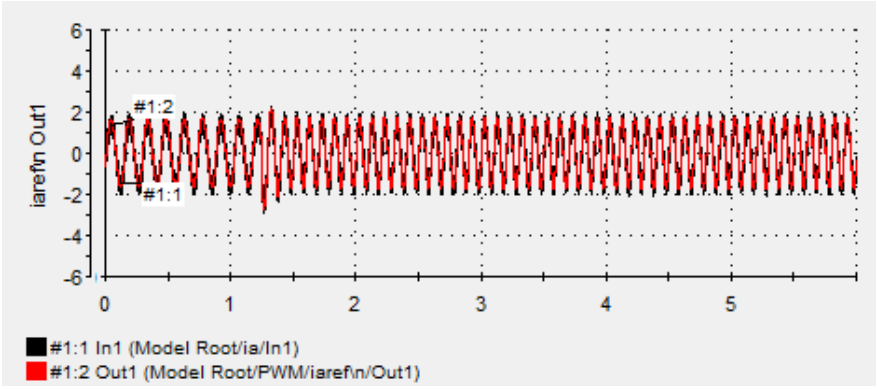

(C)

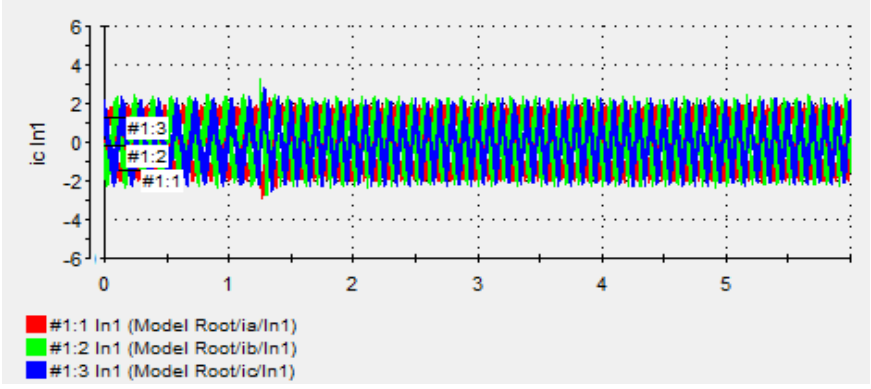

(D)

Figure 13.Speed step change of FSTPI drive at no load: (a) motor speed, (b) Speed error (c) Motor phase current,and (d) three-phase currents

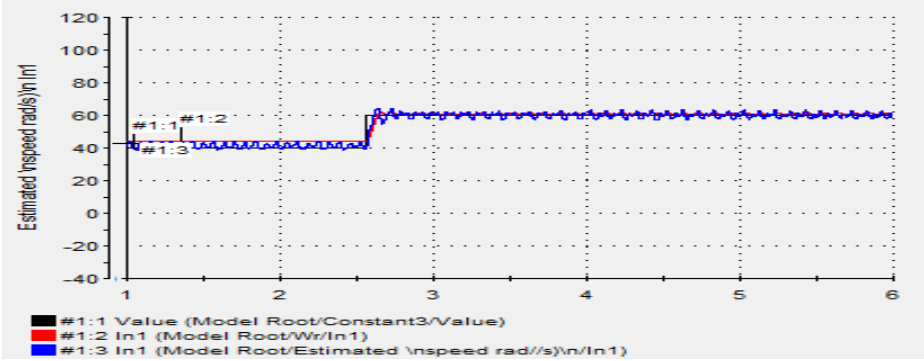

(A)

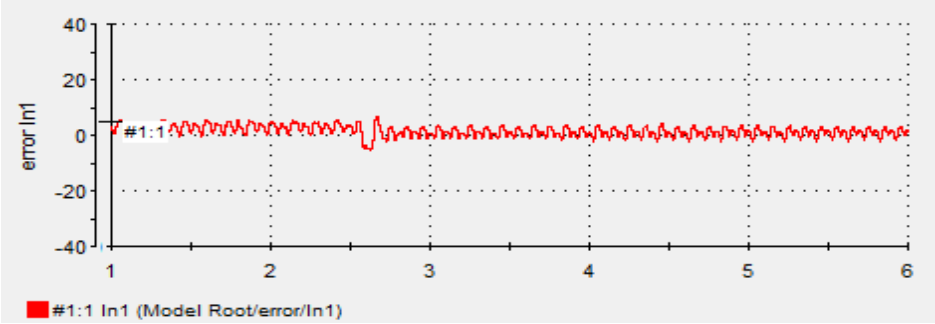

(B)

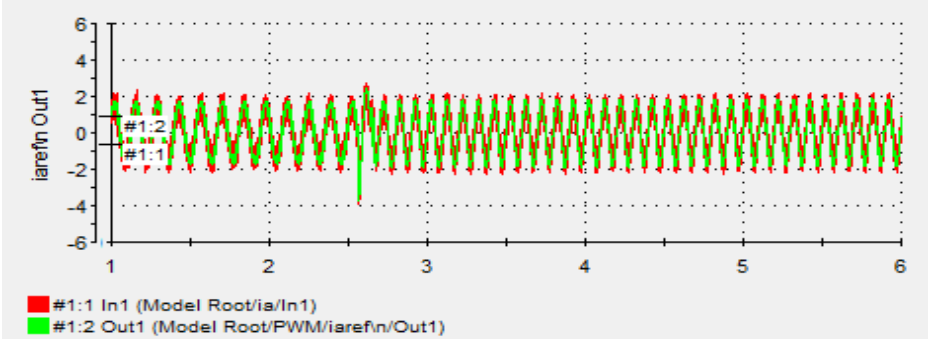

(C)

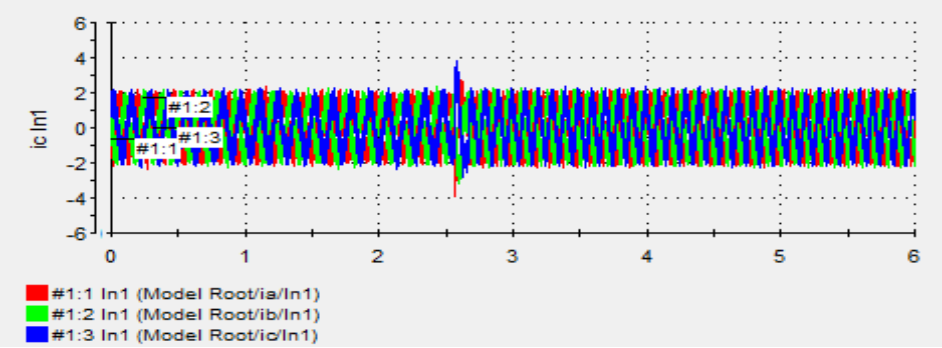

(D)

Figure 14. Experimental results of SSTPI drive at no load: (a) motor speed, (b) Speed error (c) Motor phase current,and (d) three-phase current

2.5.3. Speed step up change at very low speed from 20 to 40 rad/sec at full load

To show the drive response at very low speed, the drive is subjected to speed step up change from 20 to 40 rad/sec. Figure 15 shows the drive response when fed from FSTPI. Figure 15A shows measured and estimated speed signals with its speed reference, it's clear that the drive has good response at low speed which supports the goodness of speed estimation algorithm. Figure 15B shows nearly speed error, which mean that good speed estimation algorithm.

Figure 15C shows motor phase current, it follows its reference with good sinusoidal shape. Figure 15D shows three phase motor current. Figure 16 shows the drive response when the motor supplies from six switch three phase conventional inverter. Figure 16A shows that the estimated and measured speed follows the reference speed with nearly zero steady state error as shown in Figure 16B. Figure 16C shows the motor phase current, whereas Figure 16D shows the motor three phase currents for the step change in speed command. These results show a good correlation between the estimated speed signal and its corresponding measured as well as reference speed signals.

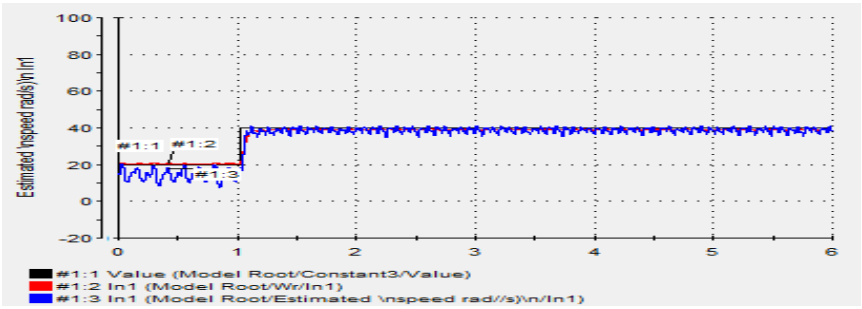

(A)

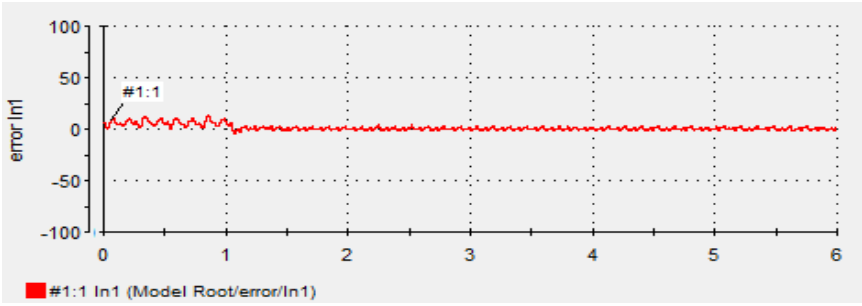

(B)

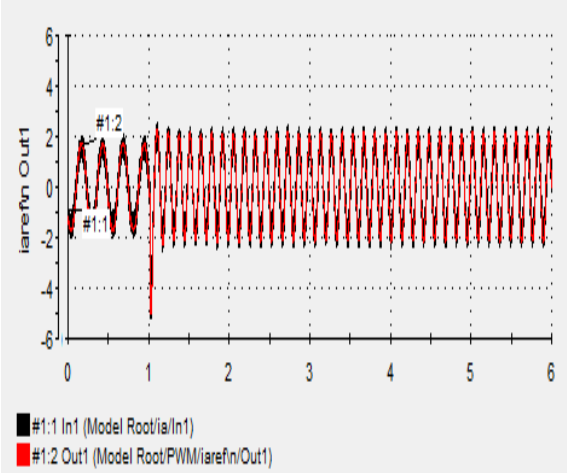

(C)

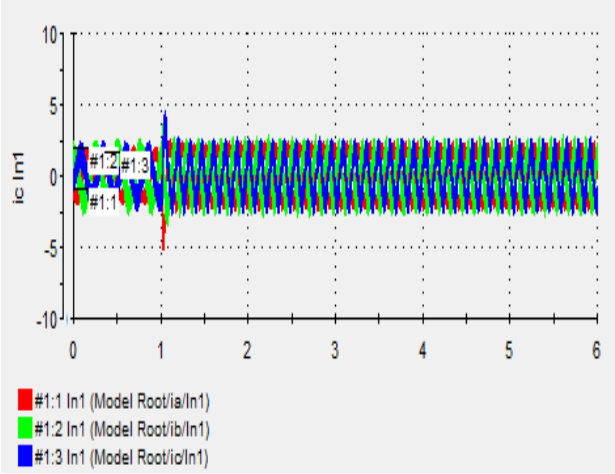

(D)

Figure 15. Experimental results of FSTPI drive at no load: (a) motor speed, (b) Speed error (c) Motor phase current, and (d) three-phase currents

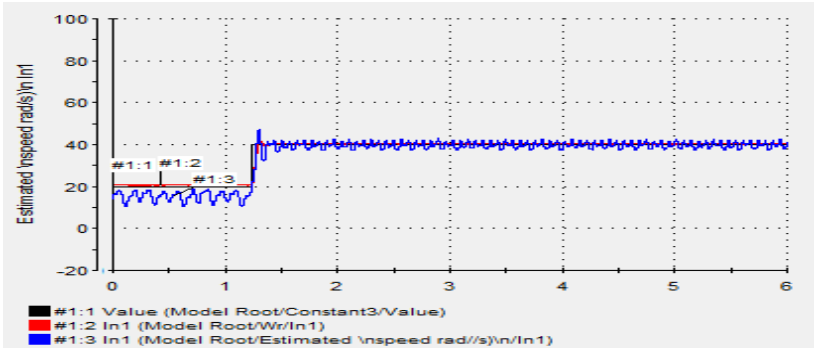

(A)

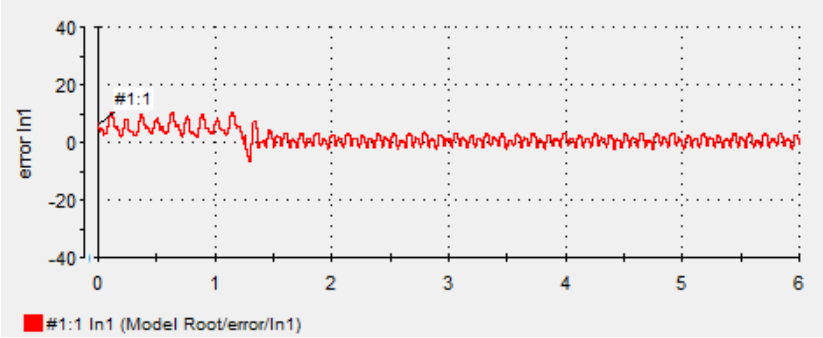

(B)

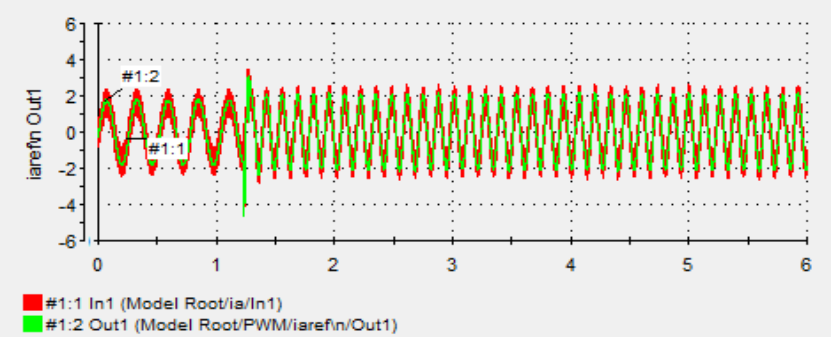

(C)

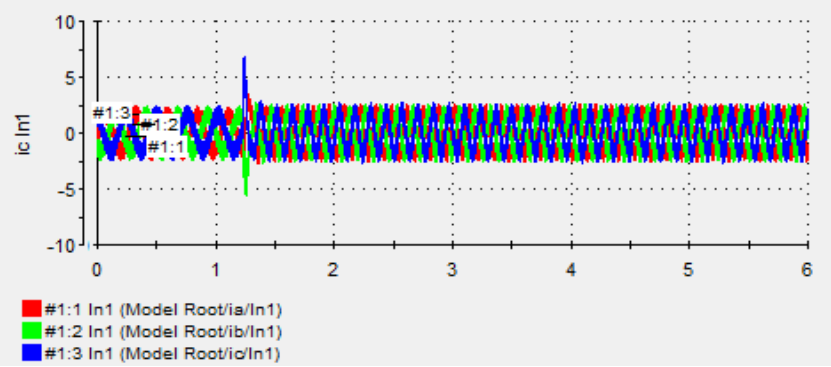

(D)

Figure 16. Experimental results of SSTPI drive at no load: (a) motor speed, (b) Speed error (c) Motor phase current, and (d) three-phase currents

3. CONCLUSION

A cost-effective FSTP inverter fed IM drive using MRAS as speed estimator has been implemented and investigated. The proposed MRAS-based FSTP inverter fed IM drive system reduces the cost of the inverter, the switching losses, the complexity of the control algorithms and increased the drive reliability of the drive compared to the conventional SSTP inverter based drive. The vector control scheme has been incorporated in the integrated drive system to achieve high performance. The MRAS as a speed estimator verified the robustness of the proposed approach. The performances of the proposed MRAS-based FSTP inverter fed IM drive has been investigated. A comparison of performances for the proposed FSTP inverter fed IM drive with a conventional SSTP inverter fed IM drive. The proposed FSTP inverter fed IM drive has been found robust and acceptable for low-cost applications such as automotive and home appliance.

REFERENCES

[1] C. B. Jacobina, *et al.*, "*Vector and Scalar Control of a Four Switch Three Phase Inverter,"* in Conf. Rec., IEEE-IAS Annul. Meeting, pp. 2422–2429, 1995.

[2] J. Holtz, "*Sensorerless Control of Induction Motor Drives,"* proceedings of IEEE, vol/issue: 90(8), pp.1359-1394, 2002.

[3] C. B. Jacobina, *et al.*, "A General PWM Strategy for Four-Switch Three-Phase Inverters," *IEEE Trans. Energy Conversion*, vol/issue: 21(4), pp. 832-838, 2006.

[4] Z. M. El-Barbary, *et al.*, "Total Harmonic Distortion Analysis of a Four Switch 3-Phase Inverter Fed Speed Sensorless Control of IM Drives," *Journal of electrical engineering*, vol. 4, 2014.

[5] N. K. Mohanty, *et al.*, "Based PWM Controlled Four Switch Three Phase Inverter Fed Induction Motor Drive," *Serbian journal of electrical engineering*, vol/issue: 7(2), pp. 195-204, 2010.

[6] J. Klima, "Analytical Investigation of an Induction Motor Fed from Four-Switch VSI with a New Space Vector Modulation Strategy," *IEEE Trans of Power Electronics*, vol/issue: 21(6), pp. 1618-1617, 2006.

[7] P. Q. Dzung, *et al*., "New Space Vector Control Approach for Four Switch Three Phase Inverter," *International Conference on Power Electronics and Drive Systems (PEDS 2007), Bangkok, Thailand*, pp. 1002–1008, 2007.

[8] J. S. Jang, *et al.*, "Sensorless Control of Four-Switch Three-Phase PMSM Drive Using Extended Kalman Filter," *IEEE*, pp.1368-1372, 2008.

[9] Prasertwong K. and Mithulananthan N., "Conventional and Fuzzy logic controllers at generator location for low frequency oscillation damping," *International Journal of Electrical Power and Energy Systems Engineering*, vol/issue: 2(3), pp. 135-143, 2009.

[10] Gowrishankar K. and Masud M.,*"MATLAB Simulink Model of Fuzzy Logic Controller with PSS and its Performance Analysis,"* IEEE-International Conference on Advances In Engineering, Science And Management, pp. 30, 31, 2012.

[11] E. Badsi, *et al.*, "DTC Scheme For A Four-Switch Inverter-Fed Induction Motor Emulating the Six-Switch Inverter Operation," *IEEE Trans. Power Electron*, vol/issue: 28(7), pp. 3528–3538, 2013.

[12] A. Khlaief, *et al*., "A Nonlinear Observer for High-Performance Sensorless Speed Control of IPMSM Drive," *IEEE Trans. Power Electronics*, vol/issue: 27(6), pp. 3028–3040, 2012.

[13] Z. M. S. El-Barbary and M. M. Elkholy, "Performance Analysis of Field Orientation of Induction Motor Drive under Open Gate of IGBT Fault," *International Journal of Power Electronics and Drive System (IJPEDS)*, vol/issue: 3(3), pp. 304~310, 2013.

[14] Y. Inoue, *et al*., "Performance Improvement of Sensorless IPMSM Drives in a Low-Speed Region Using Online Parameter Identification," *IEEE Trans. Ind. Electron*, vol/issue: 47(2), pp. 798–804, 2011.

[15] M. Hasegawa and K. Matsui, "Position Sensorless Control for Interior Permanent Magnet Synchronous Motor Using Adaptive Flux Observer with Inductance Identification," *IET Elect. Power Appl.*, vol/issue: 3(3), pp. 209–217, 2009.

[16] C. M. Ta, *et al*., *"MRAS-Based Speed Sensorless Control For Induction Motor Drives Using Instantaneous Reactive Power,"* 27th Ann. Conf. IEEE Indust. Electron. Soc. (IECON '01), vol. 2, pp. 1417–1422.

[17] S. Maiti and C. Chakraborty, "An Alternative Adaptation Mechanism for Model Reference Adaptive System Based Sensorless Induction Motor Drive," *J. Electrical. Power Components and. System*, vol/issue: 38(6), pp. 710–736, 2010.

[18] C. W. Park and W. H. Kwon, "Simple And Robust Speed Sensorless Vector Control Of Induction Motor Using Stator Current Based MRAC," *Electric Power Systems Research*, vol. 71, pp. 257–266, 2004.

APPENDIX

Machine parameters of the applied induction machine

Rated power	1.1 kw
Rated load torque	7.5 N.m.
No. of poles	4
Stator resistance	7.4826 ohm
Rotor resistance	3.6840 ohm
Rotor leakage inductance	0.0221 H
Stator leakage inductance	0.0221 H

Mutual inductance	0.4114 H
Supply frequency	50 Hz
Motor speed	1500 r.p.m.
Supply voltage	380 volts
Inertia	0.02 kg.m^2

BIOGRAPHIES OF AUTHORS

Was born in Kaferelsheihk, Egypt, in 1971. He received the B.Sc., M.Sc., and Ph.D. degrees in electrical engineering from Menoufiya University, Shebin El-Kom, Egypt, in 1994, 2002, and 2007, respectively. In 2009, he joined Kaferelsheihk University as an Assistant Professor. His research interests include AC motor drives, power electronics, and solar energy.